Temperature dependence of enhanced spin relaxation time in metallic nanoparticles: Experiment and theory

T. Koda,[1,*] S. Mitani,[2] S. Takahashi,[1,4] M. Mizuguchi,[1] K. Sato,[1] T. J. Konno,[1] S. Maekawa,[3,4] and K. Takanashi[1,†]

[1]*Institute for Materials Research, Tohoku University, Sendai 980-8577, Japan*

[2]*National Institute for Materials Science, Tsukuba 305-0047, Japan*

[3]*Advanced Science Research Center, Japan Atomic Energy Agency, Tokai 319-1195, Japan*

[4]*CREST, Japan Science and Technology Agency, Sanbancho, Tokyo 102-0075, Japan*

(Received 18 November 2012; revised manuscript received 6 December 2015; published 1 February 2016)

We study the enhanced spin relaxation time of Au nanoparticles in nanopillar-shaped double-barrier junction devices with a stacked Fe/MgO/Au-nanoparticle/MgO/Fe structure. The size of Au nanoparticles located in a current path is deduced from a transmission electron micrograph and the Coulomb blockade behavior in the current-voltage characteristics of the devices. A finite tunnel magnetoresistance (TMR) is observed above a critical current and is attributable to spin accumulation in Au nanoparticles. Based on a simple model of TMR due to spin accumulation in a nanoparticle, the spin relaxation time τ_s is estimated from the magnitude of the critical current. The temperature and bias-voltage region where TMR appears are determined from systematic observations, showing that the appearance of TMR is not associated with the Coulomb blockade but with spin accumulation. We find that the obtained τ_s is anomalously extended ($\sim$800 ns) at low temperatures and abruptly decreases above a critical temperature. Interestingly, the critical temperature strongly depends on the size of the Au nanoparticles and is much lower than the effective temperature corresponding to the discrete energy spacing. A theoretical analysis for the spin relaxation of electrons with discrete energy levels shows that not only the anomalously extended spin relaxation time, but also the strong temperature dependence of τ_s arise from the *broadening* of discrete energy levels due to coupling with phonons in the surrounding matrix. Numerical calculations using reasonable parameter values well reproduce the observed temperature and size dependence of the spin relaxation time in Au nanoparticles.

DOI: 10.1103/PhysRevB.93.085402

I. INTRODUCTION

Spin relaxation of electrons plays a crucial role in spin-related phenomena of hybrid nanostructures, such as lateral spin valve devices [1]. Spin relaxation phenomena in nanoparticles is particularly interesting because it strongly influences the spin-dependent transport in ferromagnetic double tunnel junctions via a nonmagnetic nanoparticle [2,3]. When the spin relaxation time τ_s in a nanoparticle is longer than the time interval between successive tunneling events between the top and the bottom ferromagnetic electrodes, nonequilibrium spin accumulation occurs in the nanoparticle for the antiparallel configuration of the electrode magnetization. The splitting of the spin-dependent chemical potentials due to spin accumulation suppresses the tunneling current of the junction in comparison with that of the parallel configuration, and therefore the difference in the tunneling currents between the two-magnetization configurations can be measured as the tunnel magnetoresistance (TMR). Several groups have found that the spin relaxation time is anomalously extended in various metallic nanoparticles [4–9], including not only for ferromagnetic materials (Co [4] and MnAs [8]), but also for nonmagnetic materials (Al [5], Au [6,7], and Cr [9]). In these studies, τ_s was evaluated by numerical fitting of current-voltage (I-V) characteristics using theoretical models based on spin-dependent single-electron tunneling. Another (or alternative) method for estimating τ_s is to use the relation between the τ_s and the current needed for the appearance of TMR [6]. The values of τ_s evaluated by the numerical fitting and the simple method are in fairly good agreement with each other [4]. In this simple method, τ_s is estimated from the measurement of the bias voltage dependence of MR curves using the equation $\tau_s = |e|/I_C^{TMR}$ [7,9], where e is the electron charge and I_C^{TMR} is the critical current corresponding to the voltage V_C^{TMR} for the appearance of TMR. Below V_C^{TMR}, τ_s exceeds the time interval between successive tunneling events, and TMR appears. The time interval τ_{tunnel} between successive tunneling events is inversely proportional to the magnitude of the current, i.e., $\tau_{tunnel} = |e|/I$, and can be controlled by changing bias voltage V_b.

It has been surmised that the discreteness of electronic energy levels is the main cause for large enhancement of τ_s [4,8]. The value of τ_s measured in MnAs nanoparticles, for example, is 10 μs, which is seven orders of magnitude longer than that in the bulk. In the paper about MnAs nanoparticles [8], it has been argued that the origin of the enhancement originates from the enhanced g factor induced by the discreteness of electronic energy levels although no direct evidence was provided. Here, we report on the origin of the mechanism of the enhancement of spin relaxation time; in addition, a satisfactory theoretical approach for τ_s is presented.

In this paper, the spin relaxation time τ_s in Au nanoparticles embedded in a MgO matrix was studied with varying the temperature and size of nanoparticles using a ferromagnetic double tunnel junction of Fe/MgO/Au nanoparticle/MgO/Fe. Our study reveals that τ_s is abruptly decreased at size-dependent critical temperatures, whereas it is extended up to

*Present address: AIT, Akita Research Institute of Advanced Technology, Akita 010-1623, Japan; koda@ait.pref.akita.jp

†koki@imr.tohoku.ac.jp

around 800 ns at low temperatures. A theoretical model is developed for the enhanced τ_s in a nonmagnetic nanoparticle and shows that the broadening of the discrete energy level due to coupling with phonons in the surrounding MgO matrix plays a key role in extending τ_s and its temperature dependence, leading to an understanding of spin relaxation mechanism in nanoparticles in an insulating matrix.

II. SAMPLE PREPARATION AND STRUCTURAL CHARACTARIZATION

The device structure for characterizing the electronic transport properties is schematically shown in Fig. 1(a). Ferromagnetic double tunnel junctions with Au nanoparticles embedded in a MgO tunnel barrier were prepared using molecular-beam epitaxy on polished MgO (100) single-crystal substrates with a base pressure below 1.0×10^{-7} Pa. Each layer was grown at room temperature. By adjusting each layer thickness, deposition conditions and postannealing temperatures, etc., the growth procedures in which the Au nanoparticles exhibit both the Coulomb blockade (CB) and the TMR were determined. In the devices examined, Au nanoparticles were grown on the first MgO barrier (1.5-nm thick) with a nominal thickness of 0.01 nm [7] and then were covered with the second MgO barrier (3.0-nm thick). Epitaxial growth was confirmed

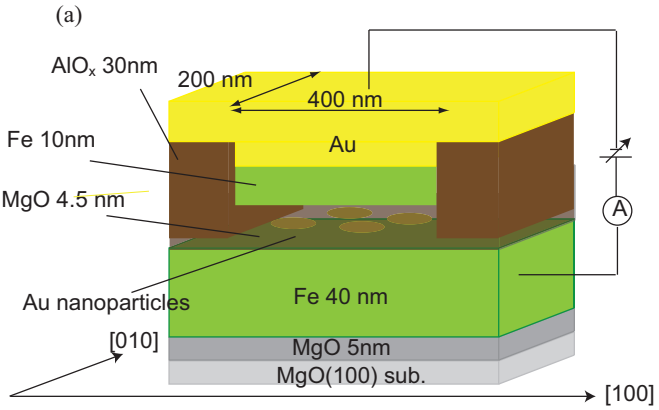

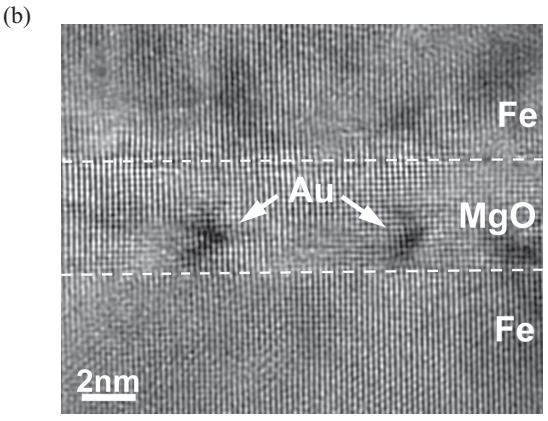

FIG. 1. (a) Device structure of a ferromagnetic double tunnel junction with Au nanoparticles grown on the first MgO barrier. (b) Aberration corrected high-resolution TEM micrograph of Au nanoparticles in a MgO tunnel barrier.

by *in situ* reflection high-energy electron diffraction. Over 100 pillars with the size of $200\times400\,\mathrm{nm}^2$ were fabricated on a substrate by electron-beam lithography and argon-ion etching techniques. The long axis of the pillars was set parallel to the Fe [100] direction, i.e., the easy magnetization axis. Electronic transport, e.g., current-voltage (I-V) curves, at temperatures ranging from 7 to 220 K was measured by using the two-terminal method. MR curves were measured in the configuration in which a magnetic field of up to 500 Oe was applied parallel to the long axis of the pillar. It is noted that specific I-V curves reflecting the Coulomb blockade effect were observed for a limited number of devices with a yield rate as low as ~10%, showing that the windows of the film growth conditions are definitely narrow. This fact suggests that natural thickness fluctuation and/or roughness of layers almost accidentally cause the restriction of the current paths needed to observe the Coulomb blockade behavior. Despite the difficulty in preparing the appropriate structure, the first observation of the Coulomb blockade using devices of a micron scale was reported in Al/SiO_2/Au or Ag nanoparticles/SiO_2/Al structures [10]. In the present study, selected films and devices (Samples A–C) were examined in detail.

A transmission electron microscopy (TEM) image of the Au nanoparticles embedded in a MgO tunnel barrier is shown in Fig. 1(b). The dark contrasts in the MgO barrier likely correspond to the Au nanoparticles. They are considered to be due to lattice strain between Au and MgO. The lattice image confirms the epitaxial growth of Au on the MgO barrier. The dark contrasts are seen with ellipsoidal shapes with an approximate diameter and height of 1 to 2 nm.

III. TEMPERATURE AND SIZE DEPENDENCE OF SPIN-DEPENDENT TRANSPORT

The I-V curves and their derivatives at various temperatures for a device (Sample A) are shown in Figs. 2(a) and 2(b). In the temperature range, single-electron tunneling behavior appears in the device due to a significant increase in charging energy when an electron tunnels into the nanoparticle [11]. The threshold voltage (V_{th}) for the Coulomb blockade shows almost identical values of about 100 mV in the temperature range. Here, V_{th} was defined as the voltage where the I-V curve starts to deviate from the linear background due to a small ohmic leak current. The Au nanoparticles were estimated to be 1.5 nm in nominal diameter from V_{th} by using the relation $V_{\mathrm{th}} = |e|/(4\pi\varepsilon_0\varepsilon_r d_{\mathrm{CB}})$ in the spherical shape approximation. Here, ε_0, ε_r, and d_{CB} are the permittivity of a vacuum, the dielectric constant of the tunnel barrier (9.8 for MgO), and the nominal diameter of the nanoparticle, respectively. The volume of the nanoparticle estimated from d_{CB} was similar to that estimated from the TEM observation. Moreover, sudden changes in the slope of the dI/dV curve at around 250 and 400 mV are observed in Fig. 2(b); these steps correspond to Coulomb staircases [2]. These results suggest that the device has a well-restricted electric current path including a single nanoparticle, even though there are several hundred Au nanoparticles in the pillar [7]. As mentioned above, the thinnest tunnel barrier area resulting from the surface roughness of the MgO layer is likely to function as the dominant current path because tunnel conductance exponentially decreases with increasing

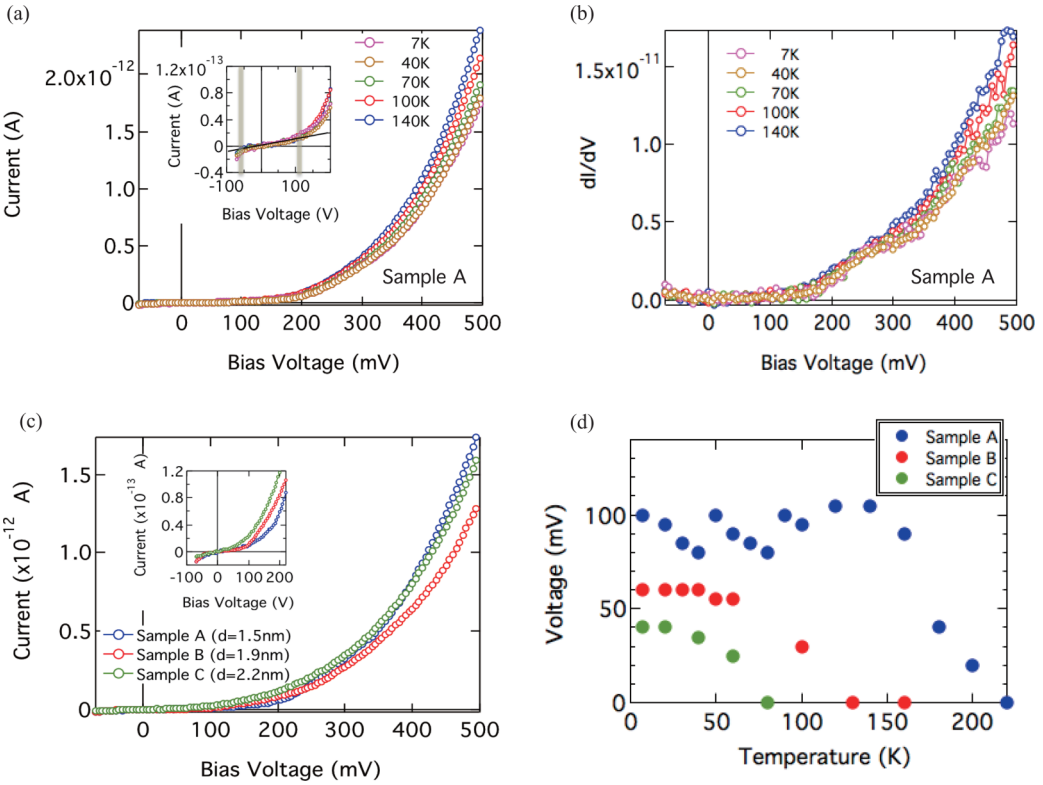

FIG. 2. (a) Current-voltage (I-V) curve of a microfabricated pillar with various temperatures. (b) dI/dV voltage of microfabricated pillar curves with various temperatures. (c) I-V curves of different samples fabricated on a substrate at 7 K. (d) Temperature dependence of the CB voltage of different samples fabricated on a substrate.

the thickness. In addition, the situation of the restricted current path is presumably unchanged within the temperature range of measurement since no significant variation was observed in the magnitude and shape of the I-V curves and their derivatives. Figure 2(c) shows three I-V curves of devices (Samples A–C) fabricated from the same substrate. These devices show single-electron tunneling behavior with the different Coulomb blockade voltages. The $V_{\rm th}$ values for Samples B and C can be determined to be roughly 60 and 40 mV, giving the $d_{\rm CB}$ of 1.9 and 2.2 nm, respectively, whereas the $d_{\rm CB}$ value is a measure in diameter that may include certain ambiguity and errors. The difference of the Au nanoparticle sizes estimated on the same substrate is considered to be due to the size distribution of Au nanoparticles grown through the natural character of the physical vapor deposition [12]. It should be noted that $V_{\rm th}$ in the I-V curve for Sample C is less clear than those for the others. Thus, we estimated the plausible threshold voltage for Sample C by taking into account the oscillation period of the dI/dV curve. It is unlikely that multiple major current paths are formed in Sample C because the tunnel current is the same order of magnitude as those in Samples A and B. We also show the temperature dependence of the CB voltage in Fig. 2(d). The threshold temperature for the appearance of the CB for the samples increased with the threshold voltage of the CB, suggesting that the estimated sample sizes reflect the relative size difference of the samples although the background charge generally affects the CB voltages.

Figure 3(a) shows the MR curves of sample A ($d_{\rm CB}$=1.5 nm) at different bias voltages and temperatures. At 7 K, TMR does not clearly appear when $V_{\rm b} \leqslant 150$ mV, whereas it definitely emerged when $V_{\rm b}$ exceeds 180 mV. Since $\tau_{\rm tunnel}$ decreases with increasing $V_{\rm b}$ and, consequently, current I of a ferromagnetic double tunnel junction, $\tau_{\rm tunnel}$ may become shorter than the spin relaxation time between $150\,{\rm mV} < V_{\rm b} \leqslant 180\,{\rm mV}$, leading to the appearance of TMR due to the spin accumulation in the nanoparticle. It should be noted that the spin accumulation in the Au nanoparticle increases gradually with the bias voltage and TMR appears stochastically when the electron in the Au nanoparticle tunnels before the spin has relaxed. Our theoretical calculation also shows the same order of magnitude in the spin relaxation time as discussed later, indicating that the simple method for the estimation of spin relaxation time captures the essential feature of the physics of spin relaxation in nanoparticles. It was also found that the bias voltage for the appearance of TMR (defined as $V_{\rm C}^{\rm TMR}$) increases with temperature as the spin relaxation time decreases with increasing temperature, resulting in a higher current required for the appearance of spin accumulation. Here, it should be noted that the anisotropic magneto-Coulomb (AMC) effect can be ruled out in the present sample. The origin of AMC is due to the anisotropy of the electrochemical potential of the ferromagnetic electrode, which is related to the magnetic anisotropy [13]. Since our sample grew epitaxially and the direction of the applied magnetic field was along the easy magnetization axis of the top and bottom Fe electrodes, the electrochemical potential of the Fe electrodes does not change with the applied magnetic field.

We also point out that those resistance changes did not correspond to the magneto-Coulomb blockade (MCB) shift. MCB is caused by the interaction between the ferromagnetic

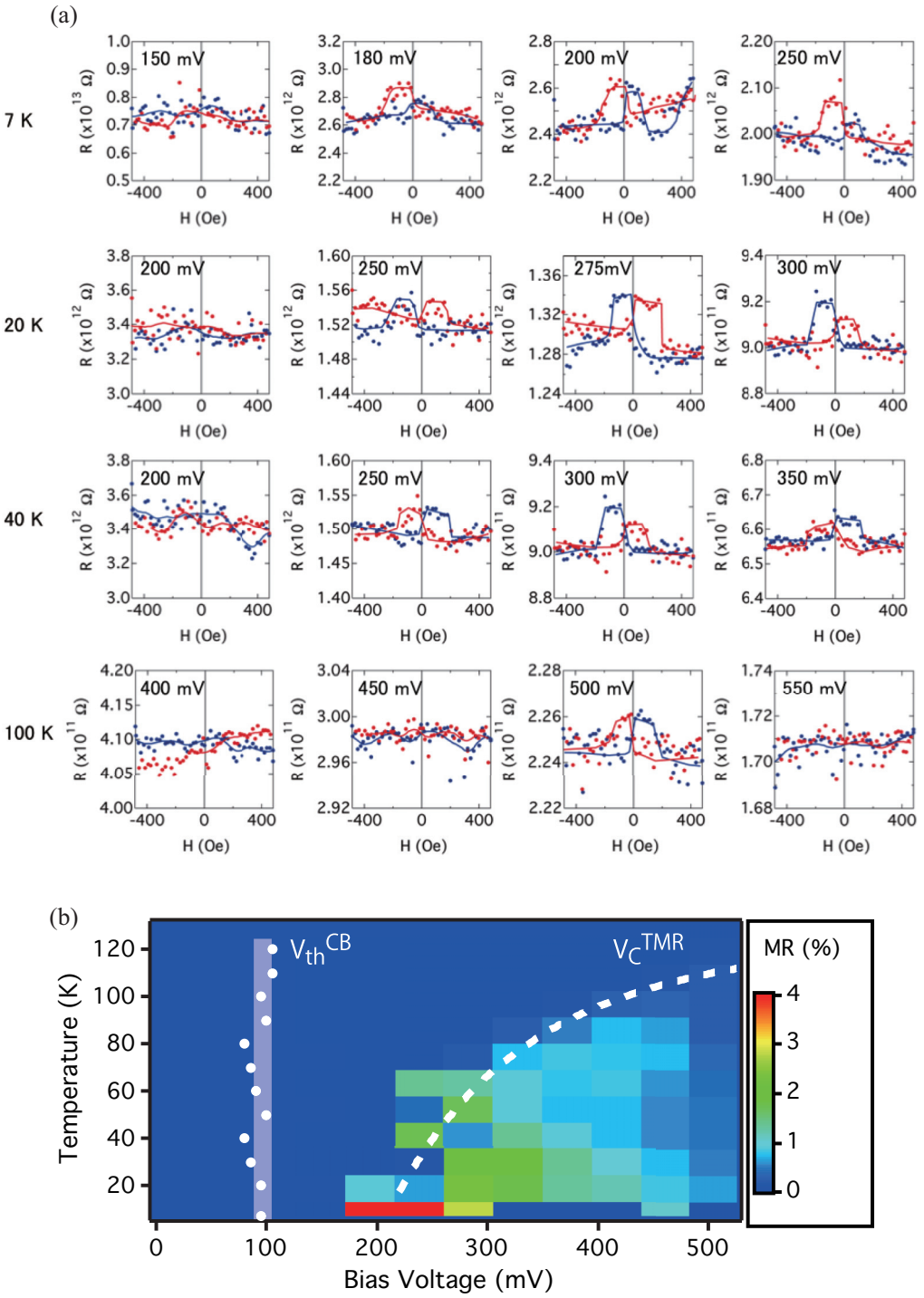

FIG. 3. (a) Bias voltage dependence of MR curves measured at 7, 20, 40, and 100 K in a device with Au nanoparticles with nominal diameters of 1.5 nm. (b) Mapping of the MR ratio as a function of temperature and bias voltage. The bias voltage V_C^{TMR} for the appearance of TMR calculated theoretically is shown by the dashed curve. The vertical dashed lines stand for the threshold bias voltage V_{th}^{CB} for the Coulomb blockade.

electrode and the nanoparticle in the double tunnel junction. The interaction causes the monotonic reduction in conductance with the magnetic field and the sudden decrease corresponding to the magnetization reversal of the ferromagnetic electrodes as explained in Ref. [14]. In addition, we confirm that the temperature dependence of the Coulomb blockade shows a different behavior compared to that of a resistance change caused by a magnetic field. Note that the MCB also cannot explain the bias voltage dependence of the MR curve in our experimental results because the MCB appears above the voltage of the Coulomb blockade. Those support our assumption that the resistance change is due to the tunnel magnetoresistance induced by the spin accumulation in the Au nanoparticle.

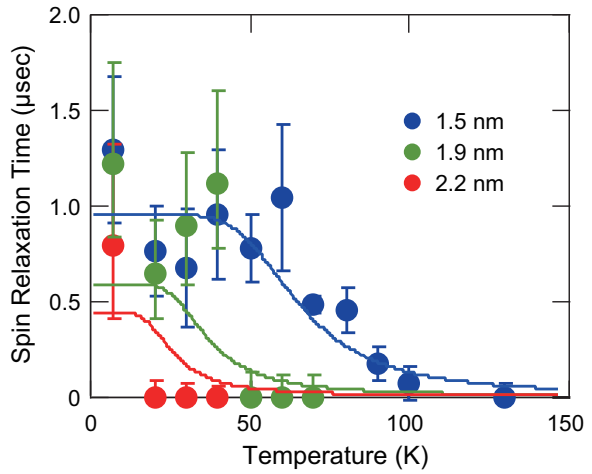

FIG. 4. Temperature dependence of the spin relaxation time of Au nanoparticles with nominal diameters of 1.5, 1.9, and 2.2 nm (blue, green, and red closed circles, respectively). The spin relaxation time τ_s at various temperatures was estimated using the equation $\tau_s = |e|/I_C^{TMR}$, where I_C^{TMR} is the current at the bias voltage for the appearance of TMR. Error bars define the range of τ_s given by the uncertainty of the bias voltage at which the MR appears in the resistance vs field measurements.

The mapping of the MR ratio as a function of temperature and bias voltage in Fig. 3(b) indicates the systematic variation of V_C^{TMR} with increasing temperature. The dashed curve for V_C^{TMR} is derived from the analysis of temperature dependence of the spin relaxation time based on a theoretical model presented in the next section. An important feature found in the mapping is that the behavior of V_C^{TMR} is clearly different from that of the Coulomb threshold voltage V_{Th}^{CB}. In addition, TMR is not observed over around 130 K whereas the Coulomb blockade is still clearly observable, indicating that the charge transport itself does not change in this temperature range and that single-electron tunneling has no specific relation with τ_s evaluated from I_C^{TMR} at V_C^{TMR}. It should be pointed out that the systematic variation of V_C^{TMR} enables us to evaluate τ_s.

The temperature dependence of τ_s evaluated for the Au nanoparticles of nominal diameters 1.5, 1.9, and 2.2 nm (blue, green, and red closed circles, respectively) is shown in Fig. 4. The solid curves are the results of the theoretical calculation in Sec. IV. The τ_s for the nominal diameters of 1.9 and 2.2 nm were estimated using the same method as that of 1.5 nm. Below 60 K, the 1.5-nm-size Au nanoparticle shows an almost constant τ_s of about 800 ns, which is much longer than that for Au bulk (the order of several hundreds of femtoseconds or shorter) [15]. It decreases rapidly with a further increase in temperature. It is not possible to estimate the spin relaxation time above 130 K because the TMR did not appear in the bias voltage range examined. In other words, τ_s above 130 K is expected to be significantly shorter and closer to that for the bulk. For the larger Au nanoparticles (i.e., $d_{CB} = 1.9$ and 2.2 nm), the temperature range in which the TMR appears is significantly reduced, that is, the critical temperature of the extended τ_s increases with the decreasing size of Au nanoparticles. In this study, some assumptions, such as the single current path and simplifications, such as the use of $\tau_s = |e|/I_C^{TMR}$ are made based on the previous studies [7,9]. The systematic results against the change in temperatures and the sizes shown in Figs. 3(b) and 4 supports the validity of the assumptions and simplifications.

IV. THEORETICAL DESCRIPTION

The obtained particle size lies within the range of large splitting of discrete electronic energy levels comparable to the thermal energy at the measurement temperatures [16,17]. A theoretical model for spin relaxation in nonmagnetic nanoparticles with discrete energy levels based on a standard approach is proposed, and an interpretation of the experimental results is presented as follows.

The spin-orbit Hamiltonian is written in the form

$$H_{SO} = \sum_{\sigma'\sigma}\sum_{mn} \langle m\sigma'|H_{SO}|n\sigma\rangle a^{\dagger}_{m\sigma'} a_{n\sigma}, \tag{1}$$

where $a^{\dagger}_{n\sigma}(a_{n\sigma})$ is the creation (annihilation) operator of an electron in state $|n\sigma\rangle$ with discrete energy ε_n and spin σ and $\langle m\sigma'|H_{SO}|n\sigma\rangle$ is the scattering amplitude of an electron from state $|n\sigma\rangle$ to state $|m\sigma'\rangle$.

The spin relaxation time τ_s is calculated using the relaxation time approximation,

$$\left(\frac{\partial s}{\partial t}\right)_{SO} = -\frac{s}{\tau_s}, \tag{2}$$

where s is the spin density accumulated in a nanoparticle, $(\partial s/\partial t)_{SO}$ is the spin relaxation rate due to spin-orbit scattering, and τ_s is the spin relaxation time. The spin density is given by

$$s = \frac{1}{2}\sum_n [f_{n\uparrow} - f_{n\downarrow}], \tag{3}$$

where $f_{n\sigma} = \langle a^{\dagger}_{n\sigma} a_{n\sigma}\rangle$ is the distribution function of an electron with discrete energy ε_n and spin σ and is given by the Fermi function with chemical potential μ_σ,

$$f_{n\sigma} = \frac{1}{e^{(\varepsilon_n - \mu_\sigma)/k_B T} + 1}. \tag{4}$$

The spin relaxation rate $(\partial s/\partial t)_{SO}$ is calculated using second-order perturbation with respect to the spin-orbit interaction [18],

$$\left(\frac{\partial s}{\partial t}\right)_{SO} = -\frac{2\pi}{\hbar}\sum_{n,m} |\langle m\downarrow|H_{SO}|n\uparrow\rangle|^2 [f(\varepsilon_n - \mu_\uparrow) - f(\varepsilon_m - \mu_\downarrow)] \frac{1}{\pi}\frac{\gamma_\varepsilon}{(\varepsilon_n - \varepsilon_m)^2 + \gamma_\varepsilon^2}, \tag{5}$$

where the δ function representing the energy conservation in an isolated system is replaced by the Lorentzian with damping γ_ε, which corresponds to the broadening of discrete energy levels caused by the coupling to thermal phonons of the surrounding insulating matrix.

When the discrete energy levels have equal spacing $\varepsilon_m = m\delta$, the spin relaxation time is calculated in the

form

$$\frac{1}{\tau_s} = \frac{2}{\pi}\frac{\delta}{\tau_{\mathrm{SO}}^*}\sum_{m=1}^{\infty}\frac{(\hbar/\tau_\varepsilon)}{\varepsilon_m^2 + (\hbar/\tau_\varepsilon)^2} = \frac{1}{\tau_{\mathrm{SO}}^*}\left(\frac{\tau_\varepsilon\delta}{\pi\hbar}\right)\left[\frac{(\pi\hbar/\tau_\varepsilon\delta)}{\tanh(\pi\hbar/\tau_\varepsilon\delta)} - 1\right], \quad (6)$$

where $1/\tau_{\mathrm{SO}}^* \equiv (4\pi/\hbar\delta)\overline{|\langle m\downarrow|H_{\mathrm{SO}}|n\uparrow\rangle|^2}$ is the characteristic spin relaxation time introduced by Kawabata [19] (the overbar denotes an average over states near the Fermi level) and $\tau_\varepsilon(=\hbar/\gamma_\varepsilon)$ is the electron lifetime of the discrete energy levels [20]. Noting that τ_{SO}^* and δ are nearly temperature independent, the observed temperature dependence of τ_s may be explained mainly by a temperature dependence of τ_ε in the discrete energy levels of the nanoparticles.

A strong temperature dependence of the electron lifetime τ_ε originates from the coupling of electrons in the nanoparticles with phonons in the surrounding insulating matrix (heat bath) and may be given by

$$\frac{1}{\tau_\varepsilon} = \frac{1}{\tau_\varepsilon^0} + \frac{1}{\tau_{\text{e-ph}}(T)}, \quad (7)$$

where τ_ε^0 is the residual electron lifetime at low temperatures presumably due to weak coupling of the nanoparticles to the outer electrodes through the insulating barriers and $\tau_{e\text{-ph}}(T)$ is the temperature-dependent lifetime due to the electron-phonon interaction between electrons in the nanoparticles and phonons in the surrounding matrix. Reflecting the population of thermal phonons in the matrix, $\tau_{\text{e-ph}}$ is proportional to $k_{\mathrm{B}}T$ at high temperatures [21] and $\exp(-\delta/k_{\mathrm{B}}T)$ at low temperatures due to the presence of the minimum excitation gap δ, resulting in strong temperature and size dependences of τ_ε. Extending the calculation of the electron lifetime in a bulk system [17,18,22] to that in a nanoparticle with a discrete electron energy spectrum, we obtain

$$\frac{1}{\tau_{\text{e-ph}}(T)} = \frac{2\pi}{\hbar}\sum_{m=1}^{m_{\mathrm{D}}}\frac{\alpha^2F(\varepsilon_m)}{\sinh(\varepsilon_m/k_{\mathrm{B}}T)}, \quad (8)$$

where α^2 is the effective electron-phonon coupling, $F(\varepsilon_m)$ is the effective phonon density of states, and the summation over the discrete levels is cut off by the Debye energy ω_{D} ($m_{\mathrm{D}} \sim \omega_{\mathrm{D}}/\delta$). Here, we assume the Debye temperature of MgO as 1000 K [23]. Using (7) and (8), we can calculate the temperature dependence of the spin relaxation time in Eq. (6). Furthermore, we can calculate the size dependence by assuming that the physical parameters depend on nanoparticle size d, $\delta \propto d^{-3}$, $\overline{|\langle m\downarrow|H_{\mathrm{SO}}|n\uparrow\rangle|^2} \propto d^{-4}$ [24,25], $1/\tau_{\mathrm{SO}}^* \propto d^{-1}$ [26], and $\alpha^2F(\varepsilon_m) = \eta S\varepsilon_m^2 \propto d^{-4}$ [27] in which η is a proportionality constant and the surface-area dependence ($S \propto d^2$) is taken into account in $F(\varepsilon_m)$.

The numerical values of τ_ε calculated from Eqs. (7) and (8) are used to derive the temperature dependence of the τ_s of the nanoparticles for the three different sizes as shown in Fig. 4. Here, the parameters of $\delta = 30.0$, 14.8, and 4.7 meV and $\tau_\varepsilon^0 = 2.2\times10^{-10}$ s for $d = 1.5$, 1.9, and 2.2 nm were used. At very low temperatures ($T \simeq 0$ K) where the level broadening is much smaller than the energy spacing ($\hbar/\tau_\varepsilon \ll \delta$), $\tau_s \approx (\tau_\varepsilon\delta/\hbar)\tau_{\mathrm{SO}}^*$ is much longer than τ_{SO}^*. As the temperature increases and level broadening becomes comparable to energy spacing $h/\tau_\varepsilon > \delta$, τ_s rapidly decreases down to τ_{SO}^*. Furthermore, the temperature range of the enhanced τ_s greatly depends on the nanoparticle size as shown with the solid curves in Fig. 4. The theoretically calculated dependence of τ_s on temperature and size qualitatively reproduces the experiment.

V. CONCLUSIONS

We systematically investigated the temperature and size dependence of extended τ_s in Au nanoparticles embedded in a MgO matrix. We revealed that the estimated spin relaxation time in Au nanoparticles showed about 800 ns at low temperatures, which is much larger than that in the bulk. We found the critical temperature above which τ_s decreased rapidly. In addition, the critical temperature also shows strong dependence on size. Our theoretical model reveals that the broadening of discrete energy levels due to coupling with phonons in the surrounding MgO matrix plays a key role in extending τ_s and its temperature dependence.

ACKNOWLEDGMENTS

The authors thank Y. Sakuraba for his support concerning the microfabrication process and setup of the measurement system. This work was supported, in part, by a Grant-in-Aid for Scientific Research in Priority Areas ("Creation and Control of Spin Current") and by a grant from the Global COE program ("Materials Integration International Center of Education Research") from the Ministry of Education, Culture, Sports, Science and Technology, Japan.

[1] F. J. Jedema, A. T. Filip, and B. J. van Wees, Nature (London) **410**, 345 (2001).
[2] H. Imamura, S. Takahashi, and S. Maekawa, Phys. Rev. B **59**, 6017 (1999).
[3] F. Ernult, K. Yakushiji, S. Mitani, and K. Takanashi, J. Phys.: Condens. Matter **19**, 165214 (2007).
[4] K. Yakushiji, F. Ernult, H. Imamura, K. Yamane, S. Mitani, K. Takanashi, S. Takahashi, S. Maekawa, and H. Fujimori, Nat. Mater. **4**, 57 (2004).
[5] Y. G. Wei, C. E. Malec, and D. Davidovic, Phys. Rev. B **76**, 195327 (2007).
[6] A. Bernand-Mantel, P. Seneor, N. Lidgi, M. Muñoz, V. Cros, S. Fusil, K. Bouzehouane, C. Deralot, A. Vaures, F. Petroff, and A. Fert, Appl. Phys. Lett. **89**, 062502 (2006).
[7] S. Mitani, Y. Nogi, H. Wang, K. Yakushiji, F. Ernult, and K. Takanashi, Appl. Phys. Lett. **92**, 152509 (2008).
[8] P. N. Hai, S. Ohya, and M. Tanaka, Nat. Nanotechnol. **5**, 593 (2010).
[9] T. Koda, S. Mitani, M. Mizuguchi, and K. Takanashi, IEEE Trans. Magn. **46**, 2060 (2010).
[10] M. Fujii, T. Kita, S. Hayashi, and K. Yamamoto, J. Phys.: Condens. Matter **9**, 8669 (1997).

[11] K. K. Likharev, Proc. IEEE **87**, 606 (1999).
[12] M. Bäumer and H. J. Freund, Prog. Surf. Sci. **61**, 127 (1999).
[13] A. Bernand-Mantel, P. Seneor, K. Bouzehouane, S. Fusil, C. Deranlot, F. Petroff, and A. Fert, Phys. Rev. B **84**, 180413(R) (2011).
[14] S. J. van der Molen, N. Tombros, and B. J. van Wees, Phys. Rev. B **73**, 220406(R) (2006).
[15] E. Montoya, B. Kardasz, C. Burrowes, W. Huttema, E. Girt, and B. Heinrich, J. Appl. Phys. **111**, 07C512 (2012).
[16] D. Davidovic and M. Tinkham, Phys. Rev. Lett. **83**, 1644 (1999).
[17] F. Kuemmeth, K. I. Bolotin, S. Shi, and D. C. Ralph, Nano Lett. **8**, 4506 (2008).
[18] S. Takahashi, T. Yamashita, H. Imamura, and S. Maekawa, J. Magn. Magn. Mater. **240**, 100 (2002).
[19] A. Kawabata, J. Phys. Soc. Jpn. **29**, 902 (1970).
[20] Y. Imry, in *Introduction to Mesoscopic Physics* (Oxford University Press, Oxford, 1997), p. 89.
[21] J. M. Ziman, *Electrons and Phonons* (Clarendon, Oxford, 1960).
[22] V. Kambersky, Czech. J. Phys. B **26**, 1366 (1976).
[23] T. H. K. Barron and J. A. Morrison, Proc. R. Soc. London, Ser. A **250**, 70 (1959).
[24] W. P. Halperin, Rev. Mod. Phys. **58**, 533 (1986).
[25] J. Buttet, R. Car, and C.W. Myles, Phys. Rev. B **26**, 2414 (1982).
[26] J. Sone, J. Phys. Soc. Jpn. **42**, 1457 (1977).
[27] D. J. Scalapino, in *Superconductivity*, edited by R. D. Parks, (Dekker, New York, 1969), p. 449.